ADVANCES IN ATMOSPHERIC SCIENCES, VOL. 40, MARCH 2023, 514–530

• **Original Paper** •

Response of the North Pacific Storm Track Activity in the Cold Season to Multi-scale Oceanic Variations of Kuroshio Extension System: A Statistical Assessment

Peilong YU[1,2], Minghao YANG[*2], Chao ZHANG[2], Yi LI[*2], Lifeng ZHANG[2], and Shiyao CHEN[2]

[1]*Collaborative Innovation Center on Forecast and Evaluation of Meteorological Disasters/Key Laboratory of Meteorological Disaster, Ministry of Education/Joint International Research Laboratory of Climate and Environment Change, Nanjing University of Information Science and Technology, Nanjing* 210044, *China*

[2]*College of Meteorology and Oceanography, National University of Defense Technology, Changsha* 410073, *China*

(Received 18 February 2022; revised 27 July 2022; accepted 25 August 2022)

ABSTRACT

In this paper, a statistical method called Generalized Equilibrium Feedback Analysis (GEFA) is used to investigate the responses of the North Pacific Storm Track (NPST) in the cold season to the multi-scale oceanic variations of the Kuroshio Extension (KE) system, including its large-scale variation, oceanic front meridional shift, and mesoscale eddy activity. Results show that in the cold season from the lower to the upper troposphere, the KE large-scale variation significantly weakens the storm track activity over the central North Pacific south of 30°N. The northward shift of the KE front significantly strengthens the storm track activity over the western and central North Pacific south of 40°N, resulting in a southward shift of the NPST. In contrast, the NPST response to KE mesoscale eddy activity is not so significant and relatively shallow, which only shows some significant positive signals near the dateline in the lower and middle troposphere. Furthermore, it is found that baroclinicity and baroclinic energy conversion play an important role in the formation of the NPST response to the KE multi-scale oceanic variations.

Key words: generalized equilibrium feedback analysis, Kuroshio Extension, multi-scale oceanic variations, North Pacific storm track

Citation: Yu, P. L., M. H. Yang, C. Zhang, Y. Li, L. F. Zhang, and S. Y. Chen, 2023: Response of the North Pacific storm track activity in the cold season to multi-scale oceanic variations of Kuroshio Extension system: A statistical assessment. *Adv. Atmos. Sci.*, **40**(3), 514−530, https://doi.org/10.1007/s00376-022-2044-z.

Article Highlights:

- The impacts of the KE multi-scale oceanic variations on NPST activity show remarkable differences.
- Baroclinicity and baroclinic energy conversion play an important role in the NPST responses to the KE multi-scale oceanic variations.
- Both large-scale and mesoscale oceanic variations of the KE system are indispensable to the mid-latitude North Pacific climate.

1. Introduction

The storm track refers to the region with the most active transient atmospheric disturbances on the synoptic scale (Blackmon, 1976), which is closely related to the cyclonic and anticyclonic paths on a daily weather map and has an indicative significance for the weather changes (Zhu and Li, 2010). Storm track plays an important role in the interplay between the tropical and mid-high latitudes through the transport of heat, moisture, and momentum and significantly impacts the maintenance of global atmospheric circulation and changes in weather and climate (Chang and Fu, 2002; Luo et al., 2011; Lee et al., 2012; Chen et al., 2020; Chu et al., 2020; Zhang et al., 2020b).

The Kuroshio Extension (KE) refers to the Kuroshio Current that breaks away from the east coast of Japan and flows into the North Pacific (Luo et al., 2016). As a continuation of the warm Kuroshio current, the KE water forms an obvious temperature difference with the near-surface cold air in the mid-latitudes, thus producing a strong ocean-to-atmosphere heat transfer. This heat release helps to maintain the surface

* Corresponding authors: Yi LI, Minghao YANG
Emails: liyi_qxxy@sina.cn, yangminghao17@nudt.edu.cn

baroclinicity and anchors energizes the overlying storm track. As a result, the KE has a robust geographic correspondence with the North Pacific storm track (NPST) (Ren et al., 2007). Tanimoto et al. (2003) pointed out that the changes in the KE sea surface temperature (SST) significantly affect the heat balance of the air-sea interface and exert an obvious thermal forcing on the atmosphere. Therefore, the KE SST should be a key factor that affects the NPST.

Since the 1990s, with the aid of high-resolution satellite data, it has been gradually recognized that the KE system presents obvious multi-scale oceanic variations, including large-scale ocean circulation variations, mesoscale oceanic fronts, and eddies. All of these oceanic variations can lead to significant SST anomalies (SSTAs) over the KE region. Specifically, the KE path clearly exhibits large-scale variations between a stable and an unstable dynamic state (Qiu et al., 2014). In its stable (unstable) state, the KE path moves northward (southward) with a lengthening (shortening) state, which tends to induce large-scale SST warming (cooling) over the KE region. Révelard et al. (2016) found that these SST changes associated with the KE large-scale variation can result in pronounced changes in North Pacific atmospheric circulation and storm track.

In contrast with the KE large-scale variation, its oceanic front primarily affects the SST in a narrow band between 34°N and 36°N (Seo et al., 2014). Although the spatial scale of SSTAs induced by the oceanic front is relatively small, they can lead to significant changes in both the near-surface air and upper atmosphere (Small et al., 2008; Kwon et al., 2010; Tao et al., 2019, 2020; Huang et al., 2020). Moreover, numerical experiments have shown that if the signal of the oceanic front is removed, the storm track activity will be significantly weakened (Nakamura et al., 2008; Sampe et al., 2010). The oceanic front can enhance the meridional temperature gradient in the near-surface atmosphere through cross-frontal differential sensible heating and thus lead to strengthened low-level atmospheric baroclinicity (Fang and Yang, 2016; Yao et al., 2020). As a result, the baroclinic eddy energy develops rapidly, and the storm track activity becomes more active (Nakamura et al., 2008; Hotta and Nakamura, 2011; Ogawa et al., 2012). Accordingly, the KE front (KEF) is supposed to be another key factor that affects the NPST, which is verified in many previous works (Kwon and Joyce, 2013; O'Reilly and Czaja, 2015; Yuan and Xiao, 2017; Zhou and Cheng, 2022).

In addition to the KEF, the KE mesoscale oceanic eddies also play an indispensable role in North Pacific ocean-atmosphere system. These fluctuations efficiently transport heat, salt, and energy in the ocean (Dong et al., 2014). Previous studies found that the KE eddy activity (KEEA) alters the poleward heat transport, leading to significant changes in the SST over the Kuroshio-Oyashio confluence region (KOCR) (Itoh and Yasuda, 2010; Sugimoto and Hanawa, 2011; Yu et al., 2020). The KE mesoscale eddies can significantly modulate the NPST activity (Sun et al., 2018). Feng et al. (2015) found that the intensified KEEA enhances the NPST. Moreover, a series of studies indicated that the existence of KE mesoscale eddies leads to a southward shift of the downstream storm track (Ma et al., 2015, 2017; Zhang et al., 2019, 2020a).

It is evident from the brief review above that both the large-scale and mesoscale oceanic variations of the KE system can have a significant effect on the NPST activity. Nevertheless, it should be noted that the KE large-scale and mesoscale variations are correlated—when the KE system is in a stable state, the KEF strengthens and shifts northward, the upstream KEEA weakens, and vice versa (Qiu and Chen, 2005, 2010). This indicates that in previous studies, the impacts of the KE large-scale (mesoscale) variation on NPST may be confused by the mesoscale (large-scale) oceanic signals. So far, the similarities and differences between the impacts of the KE multi-scale oceanic variations on NPST activity remain poorly understood and need further investigation. Resolving this issue is vital to deepening the knowledge about the mid-latitude ocean-atmosphere interaction over the North Pacific.

In the present study, we aim to separate the responses of NPST to the KE large-scale and mesoscale oceanic variations by using a statistical method called generalized equilibrium feedback analysis (GEFA; Liu et al., 2008). This method can effectively distinguish the atmospheric responses to various external forcings (Wen et al., 2015; Révelard et al., 2018). Here, we focused on the NPST responses in the cold season when the most intense air-sea interaction occurs. The remainder of the paper is organized as follows. Section 2 briefly describes the data and methods used in this study. Section 3 presents the spatial patterns of NPST responses to the KE multi-scale oceanic variations. Possible mechanisms for the impacts of the KE multi-scale oceanic variations on NPST are elucidated in section 4. A conclusion and discussion are given in section 5.

2. Data and methods

2.1. *Data*

In this study, daily atmospheric variables, including the wind speed, geopotential height, and air temperature, were used to calculate the metrics of storm track activity and associated energy conversion terms, which were provided by the ECMWF (European Centre for Medium-Range Weather Forecasts) Interim (ERA-Interim) reanalysis during the period 1982–2017 with a spatial resolution of 0.75° × 0.75° (Dee et al., 2011). The monthly surface air temperature (SAT) was obtained from the ERA-Interim reanalysis. The monthly SST data, obtained from the National Oceanic and Atmospheric Administration (NOAA) Optimum Interpolation Sea Surface Temperature (OISST) with a spatial resolution of 0.25° × 0.25° (Reynolds et al., 2007), were mainly adopted to calculate all the oceanic indices used. We also used the ERA-Interim SST product to investigate the imprints of the KE multi-scale oceanic variations on SST, consistent with the spatial resolution of relevant atmospheric responses. The daily satellite altimetry data are offered by the Archiving

Validation and Interpretation of Satellite Oceanographic (AVISO) product (Ducet et al., 2000) on a 0.25° × 0.25° grid from 1 January 1993 to 31 December 2017. The mean seasonal cycle of all variables is removed by subtracting the climatological monthly means. A cubic polynomial is also removed from each variable by employing a least squares fit to eliminate the influence of trends and ultra-low frequencies.

2.2. *SSTA index*

Following Qiu et al. (2007), the KE large-scale variation can be measured by an index defined as the average SSTA over the KE region of 32°–38°N, 142°E–180° (Fig. 1a, black box). Although this region is located to the south of maximum SST variance (Fig. 1a), the KE region possesses the strongest ocean circulation variability over the North Pacific (Fig. 1b) that primarily drives the KE SST changes (Qiu et al., 2007). Considering that the diameters of mesoscale eddies are generally less than 5°, we used a 5° × 5° spatial boxcar to filter the mesoscale SSTA from large-scale signals before calculating the KE SSTA index (Zhang et al., 2019).

2.3. *Oceanic front index*

The KEF is detected from the position of the maximum horizontal SST gradient between 32°–37°N at each longitudinal grid point from 142° to 180°E (Chen, 2008). The present paper only considers the upstream KEF position because this oceanic front becomes weak and shows obvious bifurcation in its downstream area (Kida et al., 2015). Therefore, following Seo et al. (2014), we searched the KEF in the region of 32°–37°N, 142°–155°E (Fig. 1c, black box), and the zonally averaged oceanic front position between 142°E and 155°E is defined as the KEF position (KEFP) index.

2.4. *Mesoscale eddy activity index*

We used an index to depict the intensity of the KE mesoscale eddy activity proposed by Yu et al. (2020). First, the eddy kinetic energy (EKE) in the western North Pacific is calculated according to Qiu and Chen (2005). The formula is as follows:

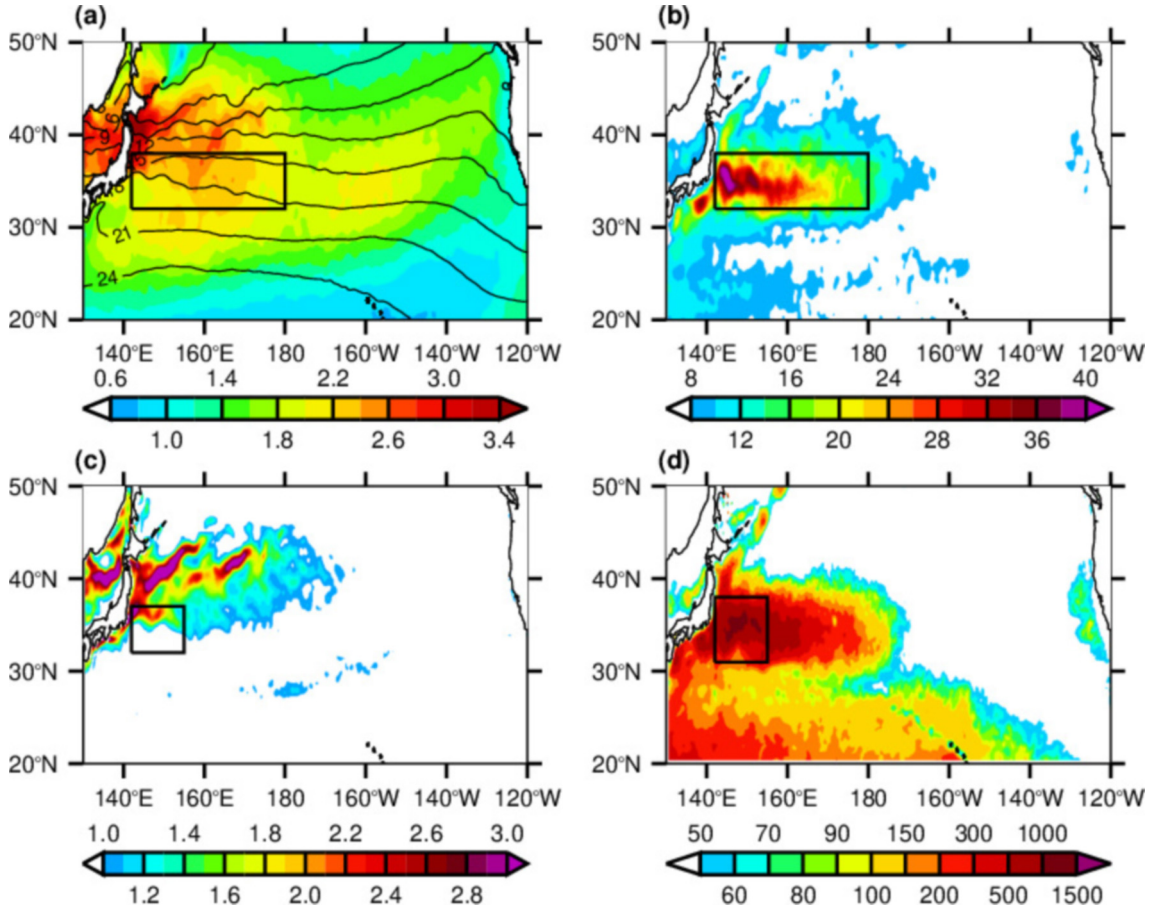

Fig. 1. (a) Climatological mean North Pacific SST (°C; black contours) in the cold season during 1982–2017. Color shading indicates the root-mean-square amplitude of SST (°C). (b) Root-mean-square amplitude of the North Pacific SSH signals (cm) in the cold season during 1993–2017. (c) Climatological mean of the magnitude of horizontal SST gradient [°C (100 km)$^{-1}$] in the cold season during 1982–2017. (d) Climatological mean surface EKE (cm^{-2} s^{-2}) in the cold season as calculated from the SSH anomalies of 1993–2017. The black boxes in four subplots denote the regions used to define the indices of the KE multi-scale oceanic variations (see text for details).

$$\mathrm{EKE} = \frac{g^2}{2f^2}\left[\left(\frac{\partial h'}{\partial x}\right)^2 + \left(\frac{\partial h'}{\partial y}\right)^2\right], \quad (1)$$

where h' denotes the high-pass filtered SSHAs that only retain changes below 300 days, g is the acceleration of gravity, and f is the Coriolis parameter. From the distribution of the EKE (see Fig. 1a of Yu et al., 2020), it can be observed that the KE EKE is the strongest in the region of 31°–38°N, 142°–155°E (Fig. 1d, black box), thus, we focus on the eddy activity in this region. Then, the KEEA index is constructed based on the KE EKE-related SSTA distribution: $\alpha T_A + \beta T_B + \gamma T_C$, where T_A, T_B, and T_C denote the normalized SST anomalies averaged over regions A (36.875°–38.375°N, 143.875°–146.125°E), B (33.625°–34.875°N, 138.375°–140.875°E), and C (34.125°–35.625°N, 148.125°–150.625°E), respectively. The coefficients α, β, and γ are obtained by the least-squares method. Specifically, the estimated EKE from the AVISO SSH data is regressed onto the normalized SSTAs from the OISST dataset, and both span the period from January 1993 to December 2017. This quantifies the EKE–SST relationship and gives a 103.98 $\mathrm{cm^{-2}\ s^{-2}}$ EKE increase per standard deviation increase in T_A, a 52.99 $\mathrm{cm^{-2}\ s^{-2}}$ EKE decrease per standard deviation increase in T_B, and a 60.25 $\mathrm{cm^{-2}\ s^{-2}}$ EKE decrease per standard deviation increase in T_C. This index actually reflects the anomalous poleward transport of warm water modulated by the KE eddy activity and highlights its climatic effects. More details about this index can be referred to in the work of Yu et al. (2020).

The temporal variations of all above-mentioned KE indices during 1982–2017 are shown in Figs. 2a–c, respectively. These indices all show obvious oscillations on interannual and decadal time scales. To focus on the cold season and increase the sample size, we selected these KE indices for September–April (SONDJFMA) (Figs. 2a–c, black dots) since the NPST responses are estimated between November and April from the KE oceanic forcings two months earlier (see details in section 2.6).

2.5. *The representation of storm track*

Since baroclinic disturbances in the mid-latitudes extend from the surface to the tropopause, the storm track can be observed at different altitudes (Chang and Fu, 2002; Gan and Wu, 2014). To study the NPST responses to the KE multi-scale oceanic variations in a more stereoscopic way, the NPST is represented by the meridional heat flux at 850 hPa, the root mean square of geopotential heights at 500 hPa, and the variance of the meridional wind velocity at 300 hPa through the use of a Lanzcos bandpass filter to isolate the synoptic-scale (2–8 day) disturbances from daily data. This method is convenient for visualizing and comparing the effects of the KE multi-scale oceanic variations on the NPST activity in the free atmosphere.

2.6. *The generalized equilibrium feedback analysis*

To distinguish the NPST responses to the KE multi-scale oceanic variations, the GEFA method developed by Liu et al. (2008) was adopted in this research, which can effectively exclude the impacts of other external forcings when revealing the atmospheric response to a certain variable (Wen et al., 2010, 2015; Wang et al., 2013; Jiang et al., 2015; Révelard et al., 2018). The basic principle is outlined as follows. Suppose the atmospheric variable $A(t)$ is at time t and the oceanic forcing $\boldsymbol{O}(t)$ has $\boldsymbol{J}$ variables, so that $\boldsymbol{O}(t) = [O_1(t), O_2(t), \cdots, O_J(t)]$. The relationship between them can be approximately expressed as:

$$A(t) = \boldsymbol{B}\boldsymbol{O}(t) + N(t), \quad (2)$$

where $\boldsymbol{B} = [B_1, B_2, \cdots, B_J]$ is a matrix containing the atmospheric response coefficients to each single oceanic variable and $N(t)$ is the internal atmospheric variability.

Owing to the poor atmospheric memory that only lasts for up to 1–2 weeks, the ocean is not affected by the atmosphere with a time lag τ larger than its intrinsic persistence. Thus, we have $\boldsymbol{C}_{ON}(\tau) \approx 0$, where $\boldsymbol{C}_{ON}(\tau)$ represents the lagged covariance matrix between $\boldsymbol{O}(t)$ and $N(t)$. By multiplying Eq. (2) by $\boldsymbol{O}(t-\tau)$ and calculating the covariance, we can obtain

$$\boldsymbol{B} = \frac{\boldsymbol{C}_{AO}(\tau)}{\boldsymbol{C}_{OO}(\tau)}. \quad (3)$$

However, considering that the atmospheric response to extratropical SSTAs needs a few months to fully develop (Ferreira and Frankignoul, 2005; Deser et al., 2007), the relation in Eq. 2 should take a more complex form. According to Frankignoul et al. (2011), $\boldsymbol{O}(t)$ in Eq. 2 can be replaced by $\boldsymbol{O}(t-d)$, where d denotes a characteristic delay time. Then, the relation in Eq. 4 becomes for $\tau > d$

$$\boldsymbol{B} = \frac{\boldsymbol{C}_{AO}(\tau)}{\boldsymbol{C}_{OO}(\tau-d)}. \quad (4)$$

To estimate the typical amplitude of the NPST response, all the oceanic time series are normalized, and thus $\boldsymbol{C}_{OO}(\tau-d)$ becomes a lag correlation matrix. Here, we chose $\tau = 2$ months, $d = 1$ month. The reasons behind the choice of these value schemes consider two aspects. 1) The atmospheric response to lower boundary forcings reaches its maximum amplitude after at least two months (Frankignoul and Sennéchael, 2007; Strong et al., 2009); 2) $\tau - d$ should be as small as possible to achieve a better condition on $\boldsymbol{C}_{OO}(\tau-d)$ to reduce the sampling errors in Eq. (5) (Liu et al., 2006). However, it should be noted that the value scheme of $\tau = d$ is not considered, for which $\boldsymbol{B}$ is divided by $\boldsymbol{C}_{OO}(0)$, and the GEFA becomes a lag regression analysis. This is because the contribution to $\boldsymbol{C}_{OO}(0)$ contains two parts, very fast changes and more persistent variability (Frankignoul et al., 2011). Considering that the NPST responses to the slow changes in boundary forcing over the KE region are our focus, $\boldsymbol{B}$ should be calculated by only using the slow contribution to $\boldsymbol{C}_{OO}(0)$, which is smaller than $\boldsymbol{C}_{OO}(0)$ itself. Hence, the use of $\boldsymbol{C}_{OO}(0)$ will underestimate the amplitudes of NPST responses. Furthermore, Révelard

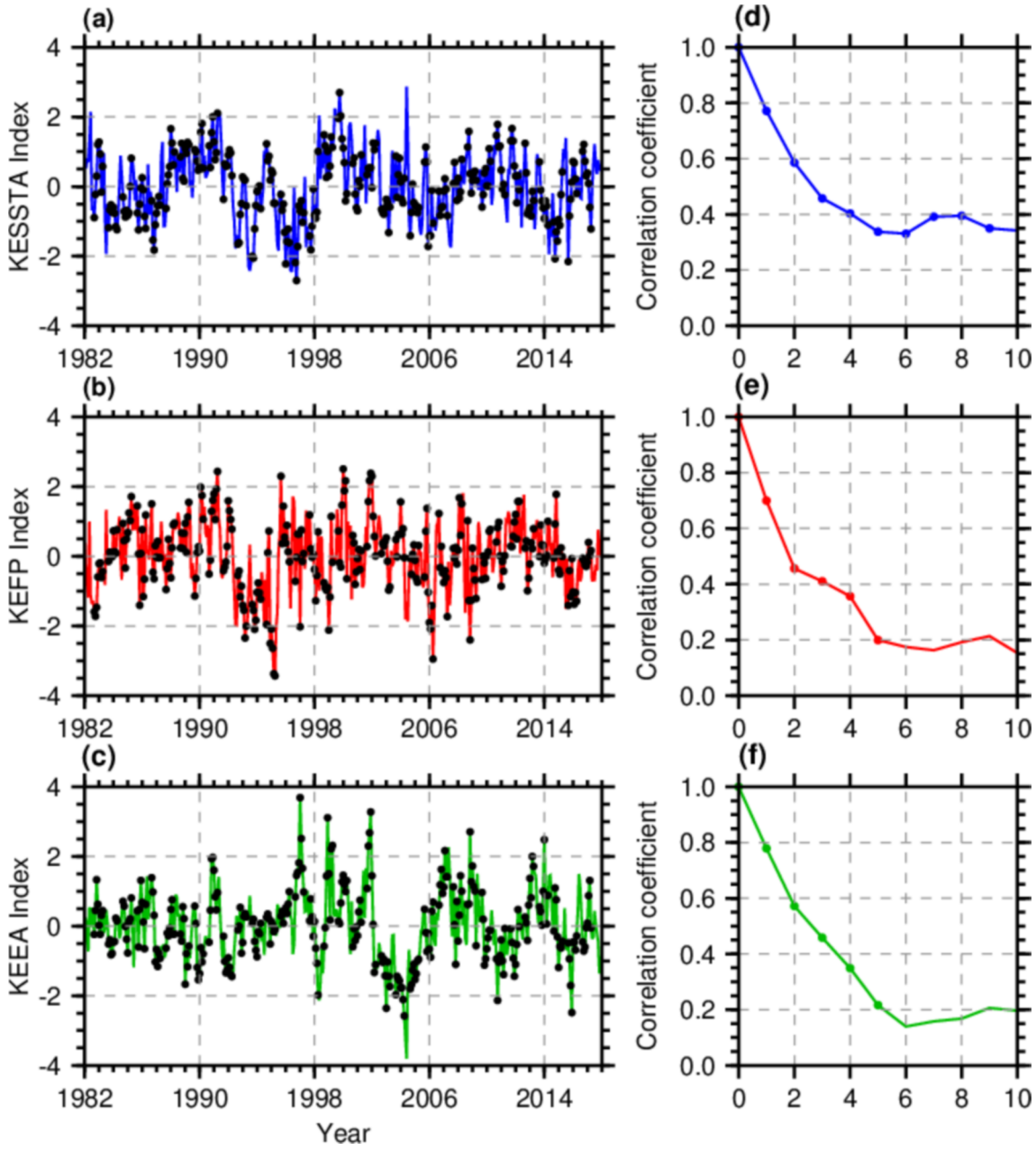

Fig. 2. Time series of the normalized (a) KE SSTA index, (b) KEFP index, and (c) KEEA index during 1982–2017. The black dots indicate the KE indices in the SONDJFMA season, as used in the GEFA. (d) Correlation coefficients of the KE SSTA index in the cold season with the KE SSTA indices of the preceding 10 months. Dots denote the correlation coefficients exceeding the 95% confidence levels. Panels (e) and (f), as in (d), but for the KEFP and KEEA indices in the cold season, respectively.

et al. (2018) adopted the GEFA with $\tau = 3$ months and $d = 1$ month to estimate the atmospheric responses by using seasonal mean anomalies, but they found that the results remain nearly the same by using monthly anomalies based on $\tau = 2$ months, $d = 1$ month. We verified, using the monthly anomalies, that the estimated responses based on $\tau = 3$ months, $d = 1$ month are largely similar to the results of the present work. All the action centers of NPST responses in lag $\tau = 2$ months can be identified in lag $\tau = 3$ months (figure not shown).

Since the tropical El Niño-Southern Oscillation (ENSO) exerts a significant impact on the mid-latitude atmosphere and ocean (Alexander et al., 2002), the first two principal components of SSTAs over the tropical Pacific between 20° S and 20°N (TP1 and TP2) are also added to the oceanic forcing matrix $\boldsymbol{O}(t)$ to avoid the interference of ENSO signals on the KE-NPST relationship. In other words, the $\boldsymbol{O}(t)$ in our study contains the time series of five indices (KE SSTA, KEFP, KEEA, TP1, and TP2). According to Révelard et al. (2018), the GEFA will be invalid if the regressors are strongly correlated, making it hard to separate their influence. Therefore, the multi-collinearity should first be exam-

ined. Table 1 shows the lag correlation matrix $\boldsymbol{C}_{OO}(\tau - d)$ used to estimate the NPST responses in the cold season. It can be clearly seen that the correlations among these five regressors are generally weak and insignificant. To better quantify the multi-collinearity, we calculated the variance inflation factors (VIFs) that are equal to the diagonal elements of the inverse correlation matrix $\boldsymbol{C}_{OO}(\tau - d)^{-1}$ (Kendall, 1946). Generally, VIFs that exceed five indicate the existence of severe multi-collinearity (Judge et al., 1988). Here, it is found that the maximum VIF of the five regressors is only 1.73. Accordingly, there is no strong problem of multi-collinearity in our study. Furthermore, the persistence of the KE large-scale SSTA index, the KEFP index, and the KEEA index is all more than five months, far exceeding the inherent atmospheric memory (Figs. 2d–f), indicating that the persistence of these oceanic forcings is in accordance with the physical basis of GEFA.

To further prove the validity of the GEFA method, the SST footprints of the KE multi-scale oceanic variations derived in two different ways are compared. Both ways use Eq. (4) to estimate the SST imprint of specific KE oceanic variation (e.g., the KE large-scale variation, KEF meridional shift, or KEEA variation). However, the first way, called univariate feedback analysis, adopts the oceanic forcing matrix $\boldsymbol{O}(t)$ that contains just only one regressor associated with this KE oceanic variation, and the second way is the GEFA utilizing the $\boldsymbol{O}(t)$ that contains all five oceanic regressors in the present study. As shown in Fig. 3 (left panels), the SST footprints derived by the univariate feedback analysis show significant remote signals beyond the definition domain of indices or regressors. For instance, all the KE indices are associated with the equatorial Pacific SSTAs, reflecting the atmospheric bridge between the equatorial and extratropical oceans. In addition, we also note that all the SSTAs associated with these KE indices show warming signals over the mid-latitude central North Pacific. However, these signals are not likely induced by the KE mesoscale oceanic variations that mainly impact the local SST, indicating the indices of KEFP and KEEA may contain the signal of the KE large-scale variation. Hence, it can be inferred that the univariate estimates of the NPST responses will be confounded by the interference of multiple oceanic forcings. In contrast, the GEFA can effectively remove the remote SST signatures of the KE multi-scale oceanic variations and lead to more localized SSTAs (Fig. 3, right panels): the SSTAs over the equatorial Pacific are largely gone, and the mid-latitude central Pacific warming associated with the KEFP and KEEA indices are also significantly weakened. We verified that these changes are mainly caused by the inclusion of ENSO indices (TP1 and TP2) in the GEFA that largely filter out the impacts of ENSO on tropical and mid-latitude SSTs. Furthermore, it is found that the SST footprints of the KE multi-scale oceanic variations derived by GEFA account for 10%–40% of the total variance over the KE region (figure not shown).

The above results indicate that GEFA is a suitable method for isolating the impacts of the KE multi-scale oceanic variations on the local SST and, thus, the NPST. The significance of each atmospheric response coefficient in $\boldsymbol{B}$ is examined using a Monte Carlo bootstrap approach (Czaja and Frankignoul, 2002), in which the GEFA is repeated 1000 times using the original oceanic time series with the atmospheric variable scrambled randomly by year, while the order of six months in the cold season of a year is retained. Then, the significance is determined at each grid by the percentage of response coefficients from the scrambled time series that are smaller in magnitude than the response coefficient from the original time series.

3. Spatial patterns for the responses of NPST to the KE multi-scale oceanic variations

3.1. *Large-scale variation*

Figure 4 shows the NPST response to the KE large-scale variation. In the lower troposphere, the NPST response mainly shows significant negative anomalies over oceanic regions southeast of Japan, in the western North Pacific between 160°E and 180°, and in the central North Pacific south of 30°N (Fig. 4a). In addition, there are a few significant positive storm track anomalies over the central North Pacific north of 40°N (Fig. 4a). This response pattern is basically similar to that of Révelard et al. (2016). In the middle troposphere, the positive storm track anomalies in the lower troposphere disappear and become significantly negative (Fig. 4b). The negative storm track anomalies become more significant to the south of Japan, the Japan Sea, and the central North Pacific, but they are no longer pronounced

Table 1. Lag correlation matrix of (left to right) the five oceanic regressors used to estimate the NPST responses in the cold season (NDJFMA). Each row and column use monthly anomalies in ONDJFM and SONDJF, respectively. The bold type denotes correlations exceeding the 95% confidence level.

	KE SSTA	KEFP	KEEA	TP1	TP2
KE SSTA	**0.81**	0.06	–0.03	–0.12	0.11
KEFP	0.19	**0.64**	0.08	**–0.24**	–0.09
KEEA	0.00	0.02	**0.76**	–0.18	0.07
TP1	**–0.25**	–0.19	–0.15	**0.98**	0.00
TP2	0.10	–0.06	0.01	–0.06	**0.93**

Maximum VIF = 1.73.

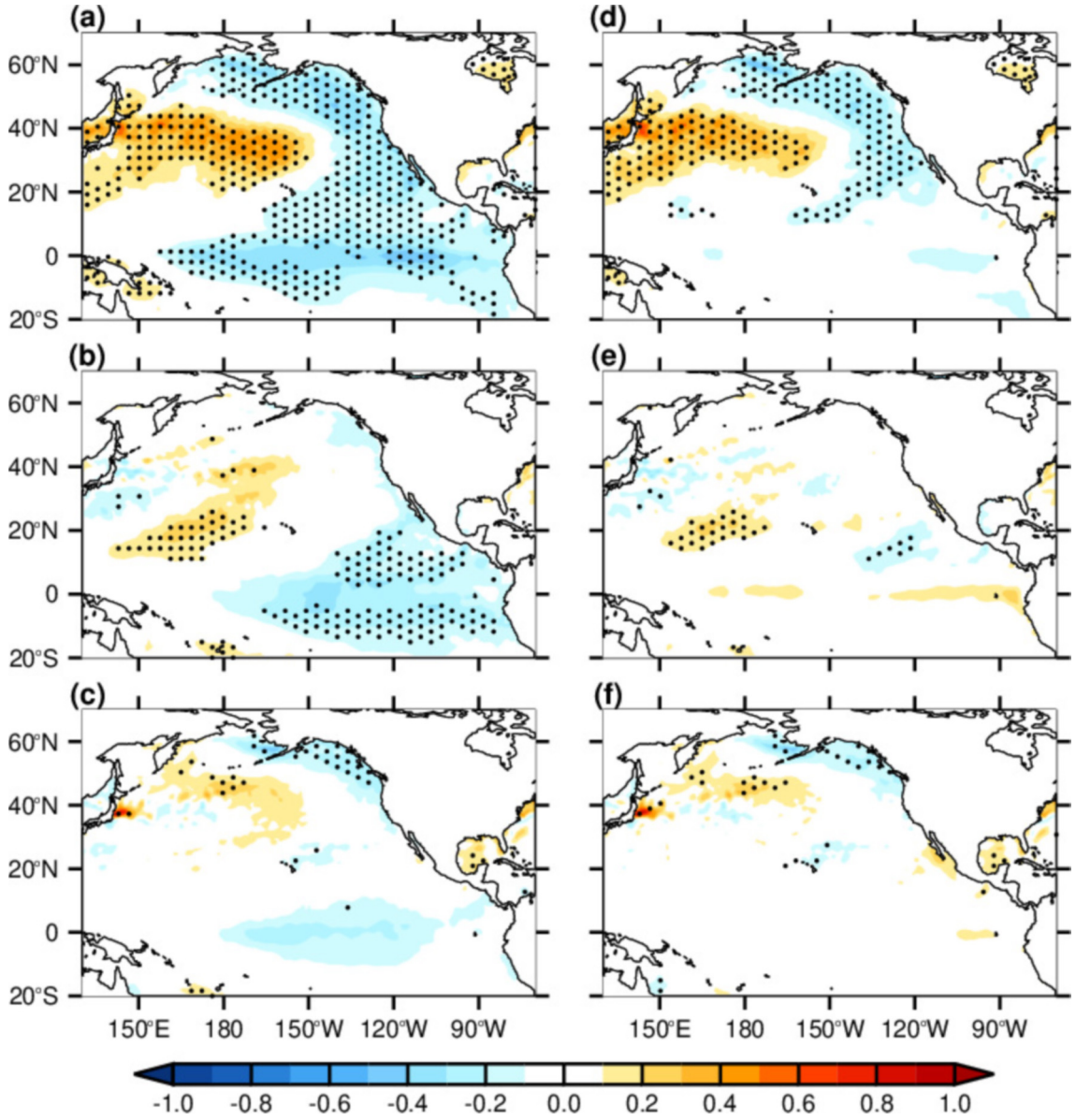

Fig. 3. SST footprints (°C) in the cold season for the (a) KE large-scale variation, (b) KEF meridional shift, and (c) KEEA variation derived by univariate feedback analysis. Panels (d)–(f), as in (a)–(c), respectively, but for the SST footprints derived by the GEFA. The stippled areas denote the 90% confidence levels based on the Monte Carlo test.

over the western North Pacific between 160°E and 180° (Fig. 4b). Compared with these storm track anomalies, significant negative storm track anomalies in the upper troposphere disappear over regions south of Japan and the central North Pacific north of 40°N and extend further eastward to the east of Japan (Fig. 4c). Some significant positive storm track anomalies also appear over the western North Pacific around 160°E (Fig. 4c). From the above analysis, it can be seen that the storm track activity is significantly weakened over the central North Pacific between 180° and 140°W south of 30°N from the lower to the upper troposphere.

3.2. *Oceanic front meridional shift*

Figure 5 shows the spatial pattern of the NPST response to the KEF meridional movement. It can be observed that the NPST response mainly presents a meridional dipole structure. In the lower troposphere, the response of the synoptic-scale meridional heat flux shows a meridional dipole pattern with positive and negative anomalies to the north and south of a nodal line at about 40°N, respectively (Fig. 5a). However, compared with the positive storm track anomalies, the significant negative anomalies are patchy. Significant positive storm track anomalies primarily appear over the western and central North Pacific between 150°E and 170°W. In the middle and upper troposphere, the NPST response pattern also exhibits a meridional dipole structure similar to that in the lower troposphere; however, the significant positive storm track anomalies appear over the central North Pacific between 170°W and 135°W, and their centers move eastward with height, indicating that

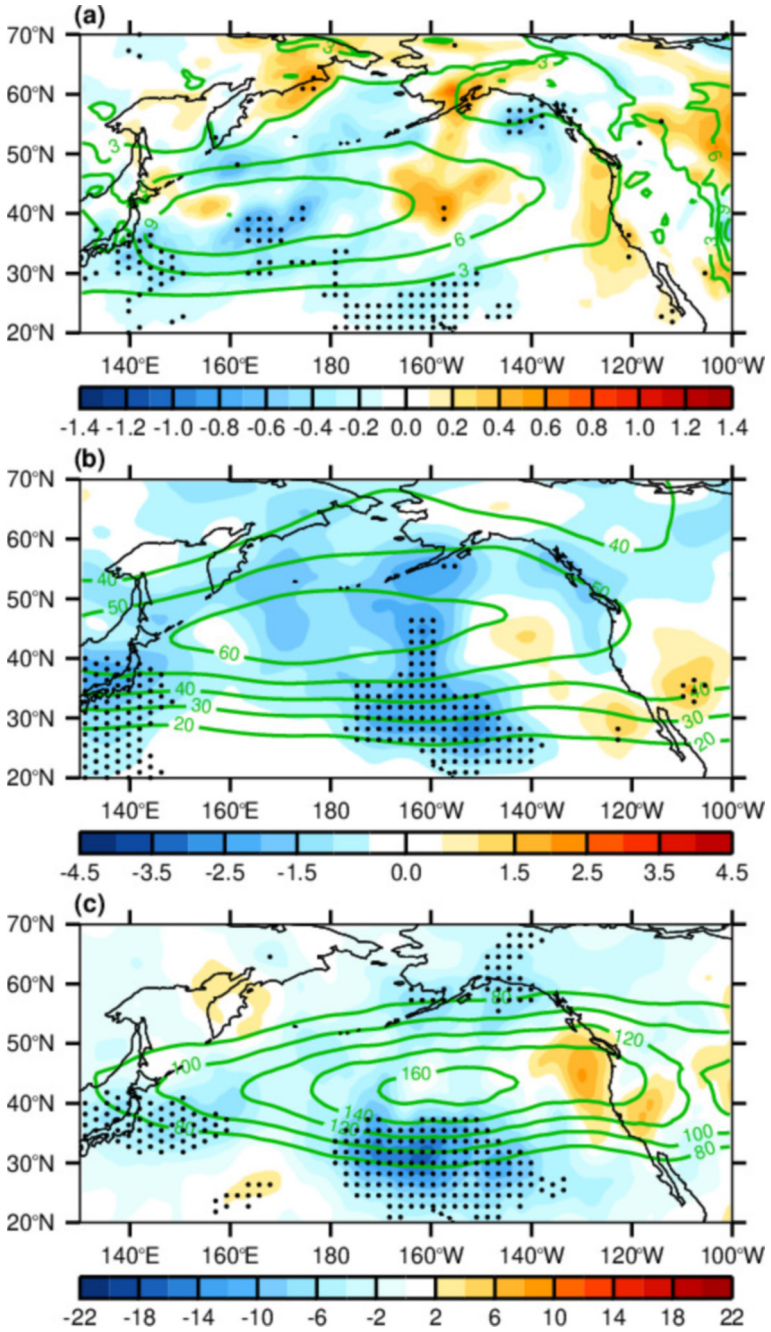

Fig. 4. Estimated response of the NPST activity represented by (a) the meridional heat flux at 850 hPa (shaded; K m s^{-1}), (b) the root-mean-square of geopotential height at 500 hPa (shaded; gpm), and (c) the variance of meridional wind velocity at 300 hPa (shaded; m^2 s^{-2}) to the KE large-scale variation. Green contours indicate the climatology with intervals of (a) 3 K m s^{-1}, (b) 10 gpm, and (c) 20 m^2 s^{-2}. The stippled areas denote the 90% confidence levels based on the Monte Carlo test.

the baroclinic waves are advected further downstream by the stronger background westerly jet at upper levels, and the negative storm track anomalies in the north become more insignificant (Figs. 5b, c). Furthermore, all the significant positive storm track anomalies from the lower to the upper troposphere are located over the southern flank of climatological NPST, indicating a southward shift of the NPST. This NPST response pattern is different from that of the KEF intensity variation exhibiting a zonal dipole structure reported by O'Reilly and Czaja (2015). Although the KEF meridional shift and intensity variation are both modulated by the KE dynamic state fluctuations as mentioned in the introduction, these two KEF variations also show obvious discrepancies (Seo et al., 2014; Bishop et al., 2015). Moreover, O'Reilly

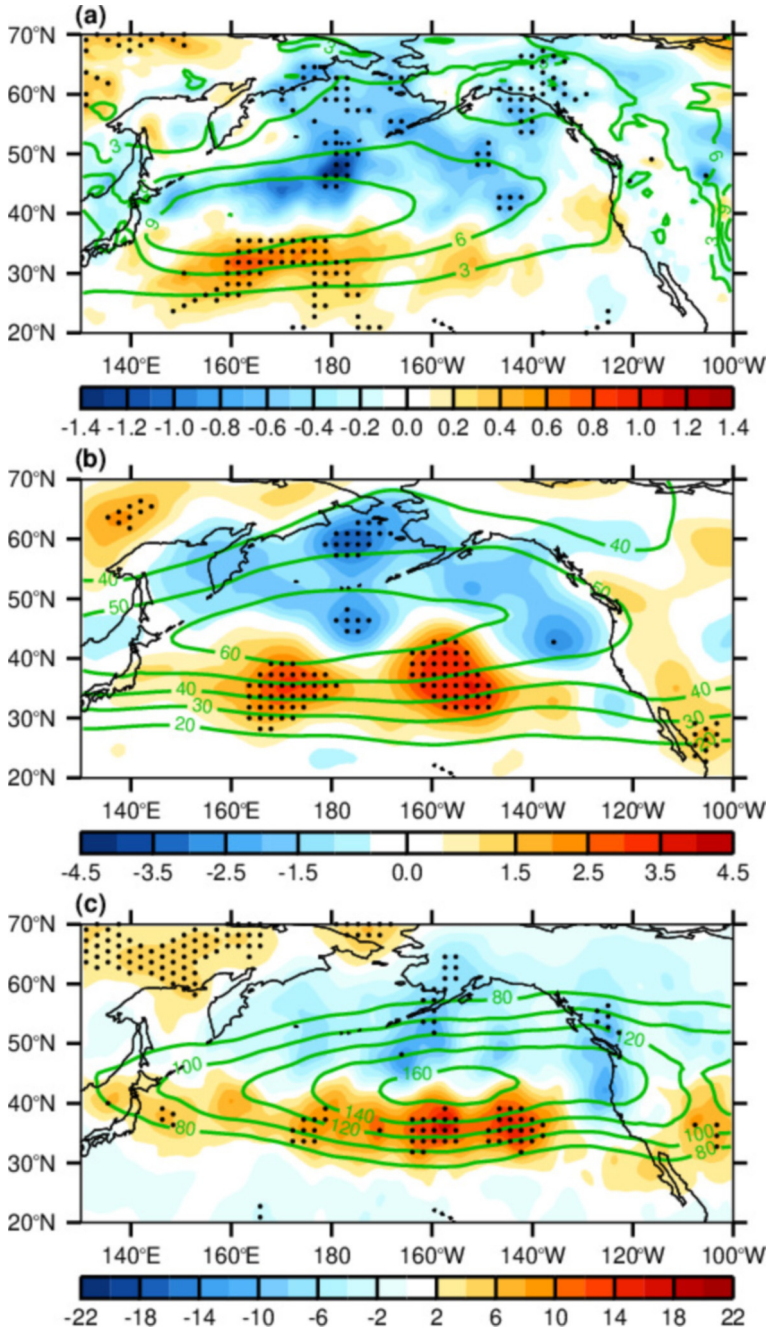

Fig. 5. As in Fig. 4, but for the estimated response of NPST activity to the KEF meridional shift.

and Czaja (2015) used unlagged composite analysis to estimate the NPST response for the study period 1992–2011, which is also different from the GEFA and temporal coverage of datasets we used. These factors may explain the differences in the results between O'Reilly and Czaja (2015) and our study.

3.3. *Mesoscale eddy activity*

At last, the NPST response to the KEEA variation is investigated. It can be found that this response also exhibits a meridional dipole structure. In the lower troposphere, negative storm track anomalies appear over the KOCR and extend northeastward (Fig. 6a), which is consistent with the findings of Bishop et al. (2015). On the southern flank of these negative anomalies, there are positive storm track anomalies extending from south Japan to the eastern North Pacific (Fig. 6a). However, the negative storm track anomalies are generally insignificant. Significant positive storm track anomalies mainly appear over the western North Pacific between 160°E and 180° and show small patchy signals over the eastern North Pacific. This dipole structure is quite similar to the NPST response pattern to the KE mesoscale SSTAs in Zhang et al. (2019). Still, the negative storm track anomalies in the north are located further south-

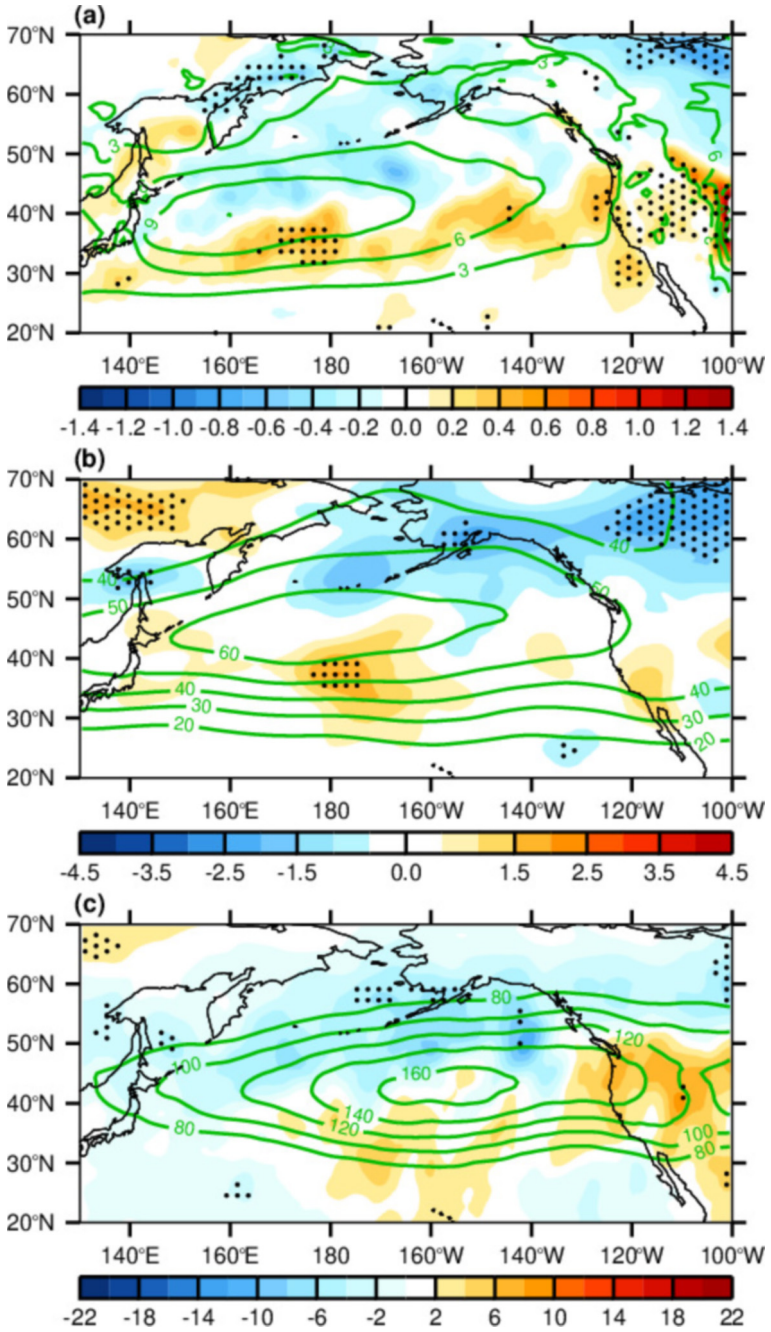

Fig. 6. As in Fig. 5, but for the estimated response of NPST activity to the KEEA variation.

ward and are insignificant. In addition, we noted that there are significantly negative and positive storm track anomalies over northern Canada and North America, respectively (Fig. 6a). These downstream responses of the storm track are also noted by Ma et al. (2017) using high-resolution model outputs but with a more northerly position. Nevertheless, the KE mesoscale SSTAs in both the works of Ma et al. (2017) and Zhang et al. (2019) include the signals of not only the oceanic front variation but also the mesoscale eddy activity, which may cause the differences in the NPST response with our study. The dipole pattern of the NPST response also remains in the middle and upper troposphere (Figs. 6b, c). However, in the middle troposphere, significant positive storm track anomalies in the lower troposphere move slightly eastward from the western North Pacific to the east of the dateline and disappear over the eastern North Pacific (Fig. 6b). Additionally, there are almost no significant storm track anomalies in the upper troposphere (Fig. 6c), indicating that the impacts of KEEA variation on the NPST are relatively shallow.

According to these results, in the cold season from the lower to the upper troposphere, the KE large-scale variation mainly leads to significant storm track anomalies over the central North Pacific south of 30°N, while the KEF meridional

shift significantly modulates the storm track activity over the western and central North Pacific south of 40°N. In contrast, the impacts of the KEEA variation on the NPST are not so significant and are relatively shallow. These KE multi-scale oceanic variations significantly capture the storm track variability over the western and central North Pacific south of 40°N, albeit with the limited explained variance of 3%–12% (figure not shown).

4. Possible mechanisms

4.1. *Surface baroclinicity*

Next, we discuss how the KE multi-scale oceanic variations modulate the NPST activity. First, the imprints of these oceanic variations on surface baroclinicity are investigated. As shown in Fig. 3d, the SST response to the KE large-scale variation shows significant basin-scale positive anomalies extending from the KE region to the central North Pacific, consistent with the results of Qiu et al. (2014) and Yu et al. (2016). These SST anomalies significantly enhance the meridional SST gradient north of about 40°N but weaken the meridional SST gradient south of about 30°N (Fig. 7a). In response to the meridional SST gradient anomalies, the meridional gradient of the low-level air temperature will also show corresponding changes due to adjustments in the atmospheric boundary layer (Sampe et al., 2010; Fang and Yang, 2016). As a result, the meridional gradient of surface air temperature (SAT) significantly decreases south of 30°N (Fig. 7b). Since the meridional SAT gradient measures the surface baroclinicity that is important for storm development, the notable decrease in meridional SAT gradient over the central North Pacific south of 30°N should be responsible for the weakened storm track activity observed there (see Figs. 4, 7b). Hereafter, only the results derived from the responses of meridional SST and SAT gradients are shown because those derived from the responses of horizontal SST and SAT gradients are virtually the same (figure not shown).

The KEF northward shift only induces local SST cooling from 142° to 155°E in two narrow latitudinal bands, one is between 36° and 40°N, and the other is between 30° and 34°N (Fig. 3e). These SST anomalies significantly enhance the meridional SST gradient in a band between 35°N and 38°N (Fig. 8a). As a result, the meridional SAT gradient and surface baroclinicity are both strengthened within this band (Fig. 8b). Compared with Fig. 5, it can be seen that the strengthened storm track activity in response to the KEF northward shift occurs near the downstream area of these surface baroclinicity changes, especially in the middle and

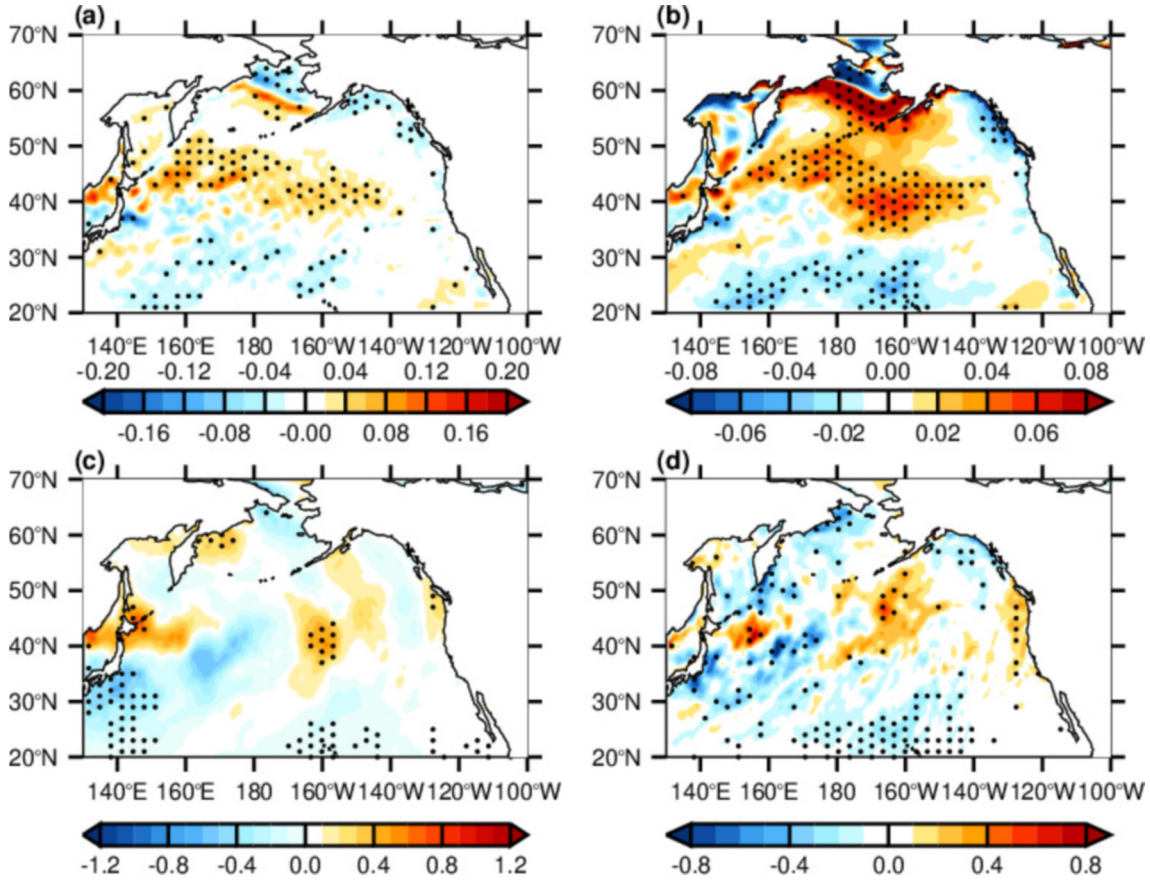

Fig. 7. (a) Estimated response of the meridional SST gradient to the KE large-scale variation [°C (100 km)$^{-1}$]. Panels (b–d), as in (a), but for the meridional SAT gradient [°C (100 km)$^{-1}$], BCEC1, and BCEC2 at 850 hPa (W m^{-2}), respectively. The stippled areas denote the 90% confidence level based on a Monte Carlo test.

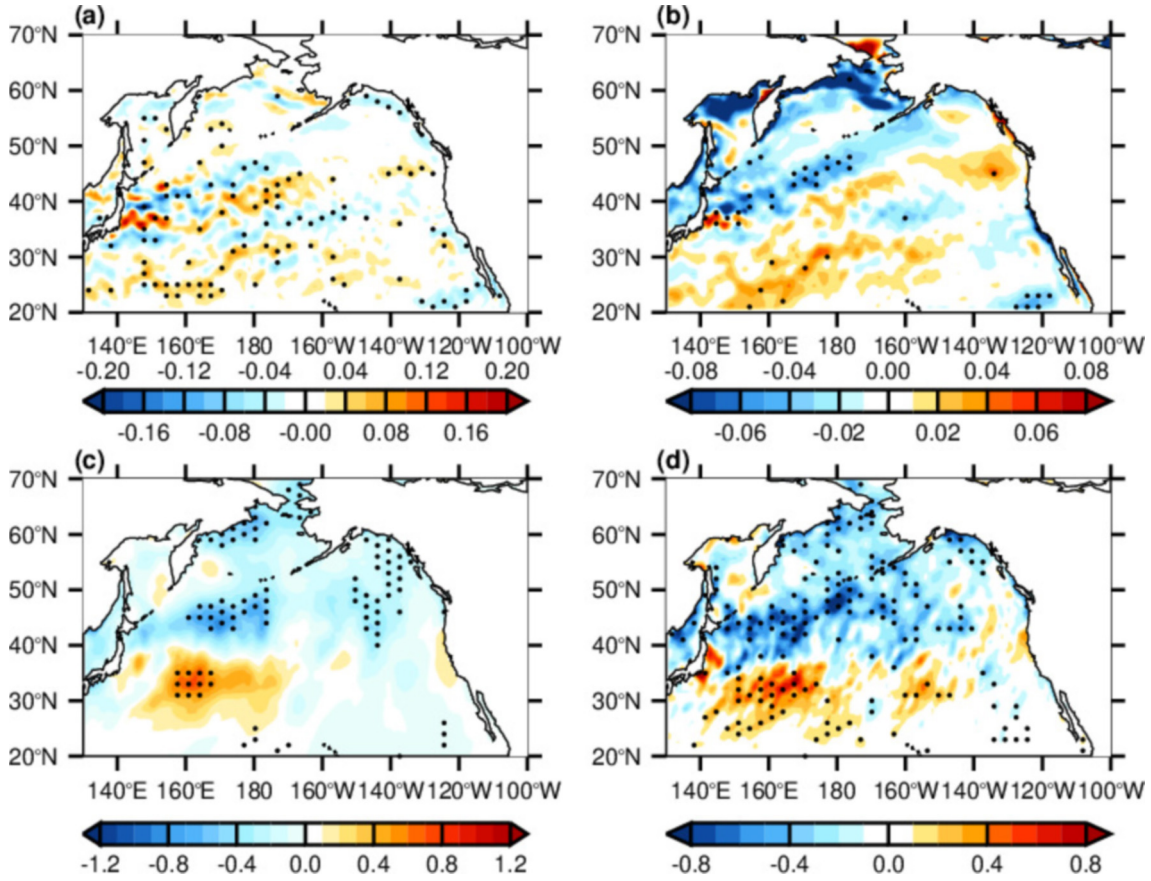

Fig. 8. As in Fig. 7, but for the estimated responses of meridional SST gradient, meridional SAT gradient, and BCEC1 and BCEC2 to the KEF meridional shift.

upper troposphere, indicative of the downstream development of storm track (Chang, 1993).

As shown in Fig. 3f, the KEEA variation leads to the significant positive SSTAs over the KOCR (36°–42°N, 142°–151°E), which has also been reported by previous studies (see introduction and references therein). Similarly, these SST anomalies significantly enhance the meridional SST gradient to the north (Fig. 9a), causing a strengthened western Oyashio front (Sugimoto et al., 2014). Correspondingly, the meridional SAT gradient, and thus the surface baroclinicity over the northern part of KOCR are intensified (Fig. 9b). Nevertheless, no significant storm track activity response is observed near this anomalous surface baroclinicity or in its nearby downstream region (see Fig. 6). This indicates that the SST imprints of KEEA over the KOCR do not seem to penetrate over the lower troposphere. Moreover, we noted that there are still some negative SSTAs to the east of KOCR between 155°E and 180° (see Fig. 3f), which may have been caused by the weakened zonal heat advection of the KE jet associated with the enhanced KEEA (Qiu et al., 2014). Since an active KEEA promotes the poleward transport of more warm water into the KOCR (e.g., Yu et al., 2020), the zonal transport of warm water to the east of this region is naturally reduced. Consequently, the negative SSTAs occur there and significantly strengthen the meridional SST gradient and surface baroclinicity to its south (Fig. 9). The position of this anomalous surface baroclinicity to the east of KOCR is more directly linked to the strengthened storm track activity near the dateline, as shown in Fig. 6. Therefore, the KEEA is supposed to impact the NPST by modulating the remote SST to the east of KOCR through an oceanic pathway.

4.2. *Baroclinic energy conversion*

Although surface baroclinicity is an effective indicator for the changes of transient eddies, baroclinic energy conversion is the main source of available potential energy that ultimately determines storm track activity (Heo et al., 2012). Therefore, to better explain the formation of the NPST response, it is necessary to diagnose and analyze the associated baroclinic energy conversion processes. Because barotropic energy conversion is approximately two orders of magnitude smaller than baroclinic energy conversion, here we only analyze the role of baroclinic energy conversion in the NPST responses to the KE multi-scale oceanic variations.

According to Cai et al. (2007), the baroclinic energy conversion from the mean available potential energy (MAPE) to the eddy available potential energy (EAPE) and from the eddy available potential energy (EAPE) to the eddy kinetic energy (EKE), denoted as BCEC1 and BCEC2, respectively. The BCEC1 and BCEC2 can be expressed as:

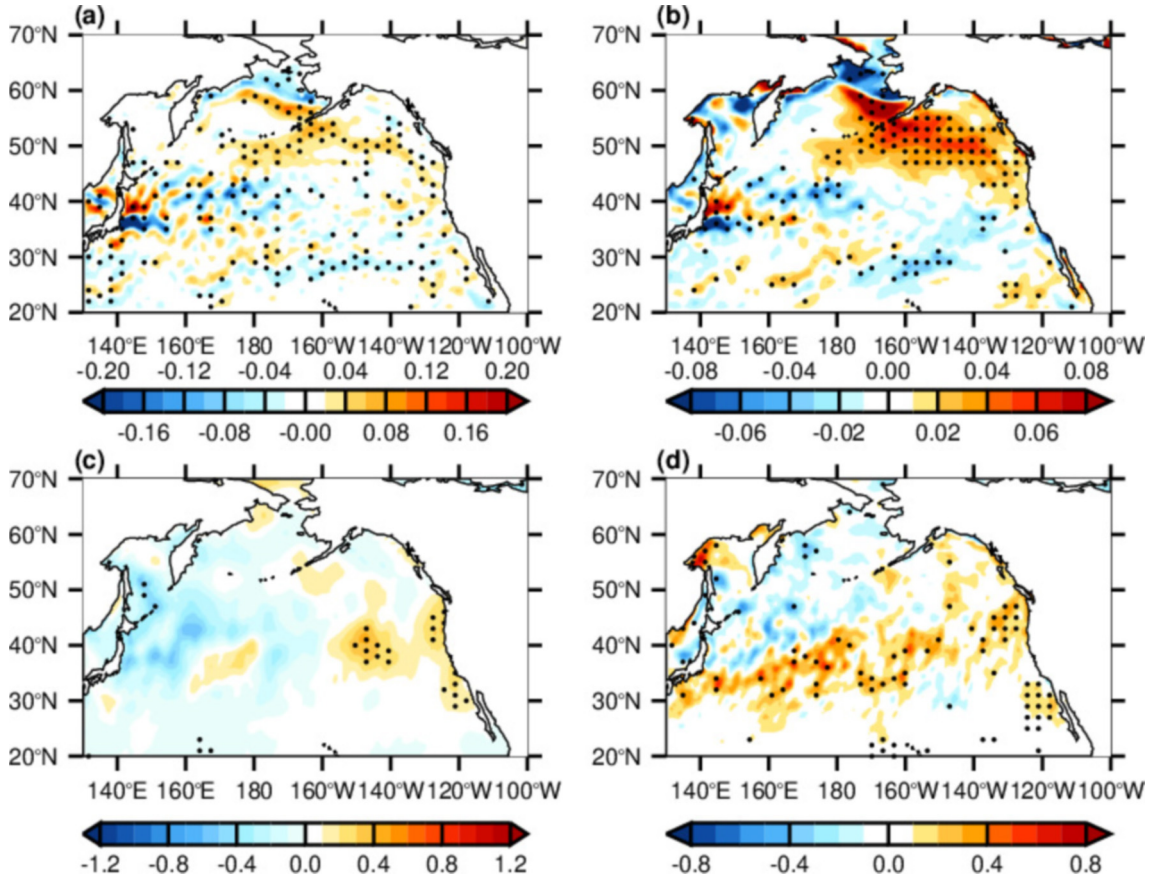

Fig. 9. As in Fig. 8, but for the estimated responses of meridional SST gradient, meridional SAT gradient, and BCEC1 and BCEC2 to the KEEA variation.

$$\mathrm{BCEC1} = -C_1\left(\frac{P_0}{p}\right)\left(-\frac{\mathrm{d}\theta}{\mathrm{d}p}\right)\left(\overline{u'T'}\frac{\partial\bar{T}}{\partial x} + \overline{v'T'}\frac{\partial\bar{T}}{\partial y}\right), \quad (5)$$

$$\mathrm{BCEC2} = -C_1\left(\overline{\omega'T}\right), \quad (6)$$

where $C_1 = (P_0/p)^{C_v/C_p}(R/g)$, g is the acceleration of gravity, P_0 is 1000 hPa, R is the gas constant for dry air, ω is the vertical velocity, $C_v(C_p)$ is the specific heat of dry air at a constant volume (pressure), and θ is the potential temperature. The overbar and the prime notations indicate the climatological average and transient disturbance, respectively.

Figures 7c, 8c, and 9c show the responses of BCEC1 over the North Pacific to the KE multi-scale oceanic variations. The BCEC1 response to the KE large-scale variation exhibits significant increases to the northeast of Hokkaido and central North Pacific, north of 40°N, and decreases to the south and southeast of Japan and central North Pacific south of 30°N (Fig. 7c). As for the BCEC1 response to the KE mesoscale oceanic processes, the KEF meridional shift leads to a significant increase over the western North Pacific south of 40°N between 155°E and 170°E and a significant decrease over the nearly the entire North Pacific north of 40°N (Fig. 8c). The KEEA variation causes a significant decrease in BCEC1 to the east of Sakhalin Island and a significant increase over the eastern North Pacific (Fig. 9c). It can be found that the above response patterns show remarkable differences with the responses of atmospheric baroclinicity (see Figs. 7b, 8b, 9b), but these differences can be understood. The fluctuations of surface baroclinicity caused by the KE oceanic forcings provide an environment favorable for the growth or decay of transient eddies. However, these modified transient eddies are not confined to the KE region, which steadily move downstream, perturb the surrounding air, and tap into or release the available potential energy from the background westerly jet along the route. This process is completely controlled by the intrinsic atmospheric variability, which helps to explain the differences in the response between BCEC1 and surface baroclinicity. Nevertheless, the changes in BCEC1 and surface baroclinicity are consistent with the significant storm track anomalies associated with the KE multi-scale oceanic variations, which are discussed in the following analysis.

In addition, the EAPE needs to be further converted into EKE to promote transient eddy motion. Equation 6 shows that the conversion of EAPE to EKE is accomplished by the rising and sinking motions of warm and cold air. The direction of energy conversion depends on the direction of the vertical motion and the thermal properties of the transient disturbance. It can clearly be seen from Figs. 7d, 8d, 9d that the BCEC2 responses to the KE multi-scale oceanic variations show a very close relationship with the spatial patterns of

NPST responses. Furthermore, compared with Figs. 7c, 8c, 9c, we note that the reduced BCEC1 in response to the KE large-scale variation contributes to a significant decrease of BCEC2 over the central North Pacific south of 30°N (see Figs. 7c, d), weakening the storm track activity there, as shown in Fig. 4. The anomalous BCEC1 induced by the KEF meridional shift tends to weaken and strengthen the BCEC2 north and south of 40°N, respectively, (see Figs. 8c, d), causing a meridional dipole structure in the NPST response (see Fig. 5). In contrast, the BCEC2 associated with the KEEA variation shows a significant increase near the dateline (Fig. 9d). As a result, more transient eddy kinetic energy occurs, leading to strengthened storm track activity there (see Figs. 6a, b). The associated local BCEC1 also increases, but the increase is not significant (Fig. 9c). This may explain why the NPST response to the KEEA variation near the dateline is not very pronounced.

Accordingly, it can be concluded that both the KE large-scale variation and KEF meridional shift alter the local SST and, thus, the surface baroclinicity. Then, the anomalous surface baroclinicity modifies the transient eddy behavior and induces a local or remote baroclinic energy conversion anomaly, which ultimately results in the formation of NPST responses to these KE oceanic variations. In contrast, the KEEA induces the remote SSTAs through an oceanic pathway, which leads to changes in the surface baroclinicity and baroclinic energy conversion, thus causing anomalous NPST activity. The above results indicate two possible pathways through which the KE multi-scale oceanic variations can impact the NPST activity.

5. Conclusion and discussion

In the present study, we used a statistical method called GEFA to elucidate the impacts of multi-scale oceanic variations of the KE system, including its large-scale variation, oceanic front meridional shift, and mesoscale eddy activity, on NPST activity from the lower to the upper troposphere in the cold season. We found that the NPST responses to these oceanic variations present remarkable differences. The KE large-scale variation significantly weakens the storm track activity over the central North Pacific south of 30°N. The KEF meridional shift significantly strengthens the storm track activity over the western and central North Pacific south of 40°N, leading to a southward shift of the NPST. In contrast, the impacts of KEEA variation on the NPST are less significant and relatively shallow, only showing some significant positive signals near the dateline in the lower and middle troposphere.

In addition, we discussed the possible mechanisms for the NPST responses to the KE multi-scale oceanic variations, focusing on surface baroclinicity and baroclinic energy conversion. Specifically, the negative SSTAs in response to the KE large-scale variation weakens the meridional SAT gradient and thus the surface baroclinicity over the central North Pacific south of 30°N, thereby favoring the weakened storm track activity observed there. The KEF northward shift enhances the local surface baroclinicity in a narrow band between 35° and 38°N, which contributes to the downstream development of storm track activity over the western and central North Pacific. In contrast, the enhanced KEEA induces remote negative SSTAs to the east of the KOCR, strengthening the surface baroclinicity to the south, thus strengthening the storm track activity near the dateline. Furthermore, to the anomalous baroclinic energy conversion agrees well with the storm track changes over these regions. These results indicate two possible pathways which contribute to the formation of NPST responses to the KE multi-scale oceanic variations. The first progression is: KE oceanic variation → local surface baroclinicity anomaly → local or remote baroclinic energy conversion anomaly → NPST anomaly, through which both the KE large-scale variation and KEF meridional shift impact the NPST activity. The second pathway describes how the KEEA modulates the NPST activity: KE oceanic variation → remote SSTAs → remote surface baroclinicity and baroclinic energy conversion anomaly → NPST anomaly.

Nevertheless, we also noted that the KE-induced changes in BCEC2 are generally more significant than those in BCEC1 (see Figs. 8, 9). In particular, the BCEC2 response to the KEEA variation shows significant signals extending northeastward from south of Japan to the central North Pacific. In contrast, there are no significant changes in BCEC1 over these regions. Therefore, it can be inferred that the MAPE is not the only source of EAPE. Ma et al. (2015, 2017) pointed out that the EAPE can also be derived from diabatic sources in addition to the MAPE in a moist atmosphere. The moist baroclinic instability is a key factor that modulates the NPST response to the KE mesoscale SSTAs. However, this mechanism is not considered here because it is difficult to diagnose from the observational and reanalysis data. Therefore, the reasons for the NPST responses to the KE multi-scale oceanic variations should be further checked and investigated using high-resolution, coupled ocean-atmosphere models (Liu et al., 2022).

Furthermore, this study only focuses on the atmospheric synoptic transient eddy activity. However, the intraseasonal (or low-frequency) transient eddies are also indispensable for large-scale atmospheric circulation and climate (Dai et al., 2021). The impacts of the KE multi-scale oceanic variations on these eddies are still unknown. Resolving this issue is important in deepening the understanding of the climatic effects of the KE system and must be addressed in future studies.

Acknowledgements. The authors sincerely acknowledge Prof. Huijun WANG, Haibo HU, and two anonymous reviewers whose valuable and insightful comments greatly improved the quality of this manuscript. This work is jointly supported by the National Natural Science Foundation of China (Grant Nos. 42105066, 42088101, 41975066). Peilong YU is supported by the China Postdoctoral Science Foundation (2021M701754), the Postdoctoral Research Funding of Jiangsu Province (2021K052A), and

the Research Project of the National University of Defense Technology (ZK20-45).

REFERENCES

Alexander, M. A., I. Bladé, M. Newman, J. R. Lanzante, N.-C. Lau, and J. D. Scott, 2002: The atmospheric bridge: The influence of ENSO teleconnections on air–sea interaction over the global oceans. *J. Climate*, **15**, 2205–2231, https://doi.org/10.1175/1520-0442(2002)015<2205:TABTIO>2.0.CO;2.

Bishop, S. P., F. O. Bryan, and R. J. Small, 2015: Bjerknes-like compensation in the wintertime North Pacific. *J. Phys. Oceanogr.*, **45**, 1339–1355, https://doi.org/10.1175/JPO-D-14-0157.1.

Blackmon, M. L., 1976: A climatological spectral study of the 500 mb geopotential height of the Northern Hemisphere. *J. Atmos. Sci.*, **33**, 1607–1623, https://doi.org/10.1175/1520-0469(1976)033<1607:ACSSOT>2.0.CO;2.

Cai, M., S. Yang, H. M. Van Den Dool, and V. E. Kousky, 2007: Dynamical implications of the orientation of atmospheric eddies: A local energetics perspective. *Tellus A: Dynamic Meteorology and Oceanography*, **59**, 127–140, https://doi.org/10.1111/j.1600-0870.2006.00213.x.

Chang, E. K. M., 1993: Downstream development of baroclinic waves as inferred from regression Analysis. *J. Atmos. Sci.*, **50**, 2038–2053, https://doi.org/10.1175/1520-0469(1993)050<2038:DDOBWA>2.0.CO;2.

Chang, E. K. M., and Y. F. Fu, 2002: Interdecadal variations in Northern Hemisphere winter storm track intensity. *J. Climate*, **15**, 642–658, https://doi.org/10.1175/1520-0442(2002)015<0642:IVINHW>2.0.CO;2.

Chen, L. L., J. B. Fang, and X.-Q. Yang, 2020: Midlatitude unstable air-sea interaction with atmospheric transient eddy dynamical forcing in an analytical coupled model. *Climate Dyn.*, **55**, 2557–2577, https://doi.org/10.1007/s00382-020-05405-0.

Chen, S. M., 2008: The Kuroshio Extension Front from satellite sea surface temperature measurements. *Journal of Oceanography*, **64**, 891–897, https://doi.org/10.1007/s10872-008-0073-6.

Chu, C. J., H. B. Hu, X.-Q. Yang, and D. J. Yang, 2020: Midlatitude atmospheric transient eddy feedbacks influenced ENSO-associated wintertime Pacific teleconnection patterns in two PDO phases. *Climate Dyn.*, **54**, 2577–2595, https://doi.org/10.1007/s00382-020-05134-4.

Czaja, A., and C. Frankignoul, 2002: Observed impact of Atlantic SST anomalies on the North Atlantic Oscillation. *J. Climate*, **15**, 606–623, https://doi.org/10.1175/1520-0442(2002)015<0606:OIOASA>2.0.CO;2.

Dai, X. L., Y. Zhang, and X.-Q. Yang, 2021: The budget of local available potential energy of low-frequency eddies in Northern Hemispheric winter. *J. Climate*, **34**, 1241–1258, https://doi.org/10.1175/JCLI-D-19-1007.1.

Dee, D. P., and Coauthors, 2011: The ERA-Interim reanalysis: Configuration and performance of the data assimilation system. *Quart. J. Roy. Meteor. Soc.*, **137**, 553–597, https://doi.org/10.1002/qj.828.

Deser, C., R. A. Tomas, and S. L. Peng, 2007: The transient atmospheric circulation response to North Atlantic SST and sea ice anomalies. *J. Climate*, **20**, 4751–4767, https://doi.org/10.1175/JCLI4278.1.

Dong, C. M., J. C. McWilliams, Y. Liu, and D. K. Chen, 2014: Global heat and salt transports by eddy movement. *Nature Communication*, **5**, 3294, https://doi.org/10.1038/ncomms4294.

Ducet, N., P. Y. Le Traon, and G. Reverdin, 2000: Global high-resolution mapping of ocean circulation from TOPEX/Poseidon and ERS-1 and -2,. *J. Geophys. Res.: Oceans*, **105**, 19477–19498, https://doi.org/10.1029/2000JC900063.

Fang, J. B., and X.-Q. Yang, 2016: Structure and dynamics of decadal anomalies in the wintertime midlatitude North Pacific ocean–atmosphere system. *Climate Dyn.*, **47**, 1989–2007, https://doi.org/10.1007/s00382-015-2946-x.

Feng, S. H., D. H. Luo, and L. H. Zhong, 2015: The relationship between mesoscale eddies in the Kuroshio Extension region and storm tracks in the North Pacific. Chinese Journal of Atmospheric Sciences, **39**, 861–874. (in Chinese with English abstract)

Ferreira, D., and C. Frankignoul, 2005: The transient atmospheric response to midlatitude SST anomalies. *J. Climate*, **18**, 1049–1067, https://doi.org/10.1175/JCLI-3313.1.

Frankignoul, C., and N. Sennéchael, 2007: Observed influence of North Pacific SST anomalies on the atmospheric circulation. *J. Climate*, **20**, 592–606, https://doi.org/10.1175/JCLI4021.1.

Frankignoul, C., N. Sennéchael, Y.-O. Kwon, and M. A. Alexander, 2011: Influence of the meridional shifts of the Kuroshio and the Oyashio Extensions on the atmospheric circulation. *J. Climate*, **24**, 762–777, https://doi.org/10.1175/2010JCLI3731.1.

Gan, B. L., and L. X. Wu, 2014: Centennial trends in Northern Hemisphere winter storm tracks over the twentieth century. *Quart. J. Roy. Meteor. Soc.*, **140**, 1945–1957, https://doi.org/10.1002/qj.2263.

Heo, K.-Y., K.-J. Ha, and S.-S. Lee, 2012: Warming of western North Pacific Ocean and energetics of transient eddy activity. *Mon. Wea. Rev.*, **140**, 2860–2873, https://doi.org/10.1175/MWR-D-11-00256.1.

Hotta, D., and H. Nakamura, 2011: On the significance of the sensible heat supply from the ocean in the maintenance of the mean baroclinicity along storm tracks. *J. Climate*, **24**, 3377–3401, https://doi.org/10.1175/2010JCLI3910.1.

Huang, J., Y. Zhang, X.-Q. Yang, X. J. Ren, and H. B. Hu, 2020: Impacts of North Pacific subtropical and subarctic oceanic frontal zones on the wintertime atmospheric large-scale circulations. *J. Climate*, **33**, 1897–1914, https://doi.org/10.1175/JCLI-D-19-0308.1.

Itoh, S., and I. Yasuda, 2010: Characteristics of mesoscale eddies in the Kuroshio–Oyashio Extension region detected from the distribution of the sea surface height anomaly. *J. Phys. Oceanogr.*, **40**, 1018–1034, https://doi.org/10.1175/2009JPO4265.1.

Jiang, Z. H., Y. Z. Wu, Z. Y. Liu, N. Wen, and C. Zhao, 2015: A diagnostic analysis of air temperature anomaly mode over China in 2009/2010 winter based on generalized equilibrium feedback assessment (GEFA) method. *Journal of Tropical Meteorology*, **21**, 121–130, https://doi.org/10.16555/j.1006-8775.2015.02.003.

Judge, G. G., R. C. Hill, W. E. Griffiths, H. Lütkepohl, and T.-C. Lee, 1988: *Introduction to the Theory and Practice of Econometrics.* 2nd ed., John Wiley and Sons, 1056 pp.

Kendall, M. G., 1946: *The Advanced Theory of Statistics*. Charles Griffin and Co, 521 pp.

Kida, S., and Coauthors, 2015: Oceanic fronts and jets around Japan: A review. *Journal of Oceanography*, **71**, 469–497, https://doi.org/10.1007/s10872-015-0283-7.

Kwon, Y.-O., and T. M. Joyce, 2013: Northern Hemisphere winter atmospheric transient eddy heat fluxes and the Gulf Stream and Kuroshio–Oyashio Extension variability. *J. Climate*, **26**, 9839–9859, https://doi.org/10.1175/JCLI-D-12-00647.1.

Kwon, Y.-O., M. A. Alexander, N. A. Bond, C. Frankignoul, H. Nakamura, B. Qiu, and L. A. Thompson, 2010: Role of the Gulf Stream and Kuroshio–Oyashio systems in large-scale atmosphere–ocean interaction: A review. *J. Climate*, **23**, 3249–3281, https://doi.org/10.1175/2010jcli3343.1.

Lee, S.-S., J. Y. Lee, B. Wang, K. J. Ha, K. Y. Heo, F. F. Jin, D. M. Straus, and J. Shukla, 2012: Interdecadal changes in the storm track activity over the North Pacific and North Atlantic. *Climate Dyn.*, **39**, 313–327, https://doi.org/10.1007/s00382-011-1188-9.

Liu, L., G. H. Wang, Z. Zhang, and H. Z. Wang, 2022: Effects of drag coefficients on surface heat flux during Typhoon Kalmaegi (2014). *Adv. Atmos. Sci.*, **39**, 1501–1518, https://doi.org/10.1007/s00376-022-1285-1.

Liu, Z. Y., M. Notaro, J. Kutzbach, and N. Z. Liu, 2006: Assessing global vegetation–climate feedbacks from observations. *J. Climate*, **19**, 787–814, https://doi.org/10.1175/JCLI3658.1.

Liu, Z. Y., N. Wen, and Y. Liu, 2008: On the assessment of nonlocal climate feedback. Part I: The generalized equilibrium feedback assessment. *J. Climate*, **21**, 134–148, https://doi.org/10.1175/2007JCLI1826.1.

Luo, D. H., Y. N. Diao, and S. B. Feldstein, 2011: The variability of the Atlantic storm track and the North Atlantic Oscillation: A link between intraseasonal and interannual variability. *J. Atmos. Sci.*, **68**, 577–601, https://doi.org/10.1175/2010JAS3579.1.

Luo, D. H., S. H. Feng, and L. X. Wu, 2016: The eddy-dipole mode interaction and the decadal variability of the Kuroshio Extension system. *Ocean Dynamics*, **66**, 1317–1332, https://doi.org/10.1007/s10236-016-0991-6.

Ma, X. H., P. Chang, R. Saravanan, R. Montuoro, H. Nakamura, D. X. Wu, X. P. Lin, and L. X. Wu, 2017: Importance of resolving Kuroshio front and eddy influence in simulating the North Pacific storm track. *J. Climate*, **30**, 1861–1880, https://doi.org/10.1175/JCLI-D-16-0154.1.

Ma, X., and Coauthors, 2015: Distant influence of Kuroshio eddies on North Pacific weather patterns. *Scientific Reports*, **5**, 17785, https://doi.org/10.1038/srep17785.

Nakamura, H., T. Sampe, A. Goto, W. Ohfuchi, and S.-P. Xie, 2008: On the importance of midlatitude oceanic frontal zones for the mean state and dominant variability in the tropospheric circulation. *Geophys. Res. Lett.*, **35**, L15709, https://doi.org/10.1029/2008GL034010.

Ogawa, F., H. Nakamura, K. Nishii, T. Miyasaka, and A. Kuwano-Yoshida, 2012: Dependence of the climatological axial latitudes of the tropospheric westerlies and storm tracks on the latitude of an extratropical oceanic front. *Geophys. Res. Lett.*, **39**, L05804, https://doi.org/10.1029/2011GL049922.

O'Reilly, C. H., and A. Czaja, 2015: The response of the Pacific storm track and atmospheric circulation to Kuroshio Extension variability. *Quart. J. Roy. Meteor. Soc.*, **141**, 52–66, https://doi.org/10.1002/qj.2334.

Qiu, B., and S. M. Chen, 2005: Variability of the Kuroshio Extension jet, recirculation gyre, and mesoscale eddies on decadal time scales. *J. Phys. Oceanogr.*, **35**, 2090–2103, https://doi.org/10.1175/JPO2807.1.

Qiu, B., and S. M. Chen, 2010: Eddy-mean flow interaction in the decadally modulating Kuroshio Extension system. *Deep Sea Research Part II: Topical Studies in Oceanography*, **57**, 1098–1110, https://doi.org/10.1016/j.dsr2.2008.11.036.

Qiu, B., N. Schneider, and S. M. Chen, 2007: Coupled decadal variability in the North Pacific: An observationally constrained idealized model. *J. Climate*, **20**, 3602–3620, https://doi.org/10.1175/JCLI4190.1.

Qiu, B., S. M. Chen, N. Schneider, and B. Taguchi, 2014: A coupled decadal prediction of the dynamic state of the Kuroshio Extension system. *J. Climate*, **27**, 1751–1764, https://doi.org/10.1175/JCLI-D-13-00318.1.

Ren, X. J., X. Q. Yang, B. Han, and G. Y. Xu, 2007: North Pacific storm track variations in winter season and the coupled pattern with the midlatitude atmosphere-ocean system. *Chinese Journal of Geophysics*, **50**, 94–103, https://doi.org/10.1002/cjg2.1014. (in Chinese with English abstract)

Révelard, A., C. Frankignoul, and Y.-O. Kwon, 2018: A multivariate estimate of the cold season atmospheric response to North Pacific SST variability. *J. Climate*, **31**, 2771–2796, https://doi.org/10.1175/JCLI-D-17-0061.1.

Révelard, A., C. Frankignoul, N. Sennéchael, Y.-O. Kwon, and B. Qiu, 2016: Influence of the decadal variability of the Kuroshio Extension on the atmospheric circulation in the cold season. *J. Climate*, **29**, 2123–2144, https://doi.org/10.1175/JCLI-D-15-0511.1.

Reynolds, R. W., T. M. Smith, C. Y. Liu, D. B. Chelton, K. S. Casey, and M. G. Schlax, 2007: Daily high-resolution-blended analyses for sea surface temperature. *J. Climate*, **20**, 5473–5496, https://doi.org/10.1175/2007jcli1824.1.

Sampe, T., H. Nakamura, A. Goto, and W. Ohfuchi, 2010: Significance of a midlatitude SST frontal zone in the formation of a storm track and an eddy-driven westerly jet. *J. Climate*, **23**, 1793–1814, https://doi.org/10.1175/2009JCLI3163.1.

Seo, Y., S. Sugimoto, and K. Hanawa, 2014: Long-term variations of the Kuroshio Extension path in winter: Meridional movement and path state change. *J. Climate*, **27**, 5929–5940, https://doi.org/10.1175/JCLI-D-13-00641.1.

Small, R. J., and Coauthors, 2008: Air–sea interaction over ocean fronts and eddies. *Dyn. Atmos. Oceans*, **45**, 274–319, https://doi.org/10.1016/j.dynatmoce.2008.01.001.

Strong, C., G. Magnusdottir, and H. Stern, 2009: Observed feedback between winter sea ice and the North Atlantic Oscillation. *J. Climate*, **22**, 6021–6032, https://doi.org/10.1175/2009JCLI3100.1.

Sugimoto, S., and K. Hanawa, 2011: Roles of SST anomalies on the wintertime turbulent heat fluxes in the Kuroshio–Oyashio confluence region: Influences of warm eddies detached from the Kuroshio Extension. *J. Climate*, **24**, 6551–6561, https://doi.org/10.1175/2011JCLI4023.1.

Sugimoto, S., N. Kobayashi, and K. Hanawa, 2014: Quasi-decadal variation in intensity of the western part of the winter subarctic SST front in the western North Pacific: The influence of Kuroshio Extension path state. *J. Phys. Oceanogr.*, **44**, 2753–2762, https://doi.org/10.1175/JPO-D-13-0265.1.

Sun, X. G., L. F. Tao, and X.-Q. Yang, 2018: The influence of oceanic stochastic forcing on the atmospheric response to midlatitude North Pacific SST anomalies. *Geophys. Res. Lett.*, **45**, 9297–9304, https://doi.org/10.1029/2018GL078860.

Tanimoto, Y., H. Nakamura, T. Kagimoto, and S. Yamane, 2003:

An active role of extratropical sea surface temperature anomalies in determining anomalous turbulent heat flux. *J. Geophys. Res.: Oceans*, **108**, 3304, https://doi.org/10.1029/2002JC001750.

Tao, L. F., X. G. Sun, and X.-Q. Yang, 2019: The asymmetric atmospheric response to the midlatitude North Pacific SST anomalies. *J. Geophys. Res.: Atmos.*, **124**, 9222–9240, https://doi.org/10.1029/2019JD030500.

Tao, L. F., X.-Q. Yang, J. B. Fang, and X. G. Sun, 2020: PDO-related wintertime atmospheric anomalies over the midlatitude North Pacific: Local versus remote SST forcing. *J. Climate*, **33**, 6989–7010, https://doi.org/10.1175/JCLI-D-19-0143.1.

Wang, F. Y., Z. Y. Liu, and M. Notaro, 2013: Extracting the dominant SST modes impacting North America's observed climate. *J. Climate*, **26**, 5434–5452, https://doi.org/10.1175/JCLI-D-12-00583.1.

Wen, N., Z. Liu, and Q. Liu, 2010: Observed atmospheric responses to global SST variability modes: A unified assessment using GEFA. *J. Climate,*, **23**, 1739–1759, https://doi.org/10.1175/2009JCLI3027.1.

Wen, N., Z. Y. Liu, and Y. H. Liu, 2015: Direct impact of El Niño on East Asian summer precipitation in the observation. *Climate Dyn.*, **44**, 2979–2987, https://doi.org/10.1007/s00382-015-2605-2.

Yao, Y., Z. Zhong, X.-Q. Yang, and X. G. Huang, 2020: Future changes in the impact of North Pacific midlatitude oceanic frontal intensity on the wintertime storm track in CMIP5 models. *J. Meteor. Res.*, **34**, 1199–1213, https://doi.org/10.1007/s13351-020-0057-z.

Yu, P. L., L. F. Zhang, Y. C. Zhang, and B. Deng, 2016: Interdecadal change of winter SST variability in the Kuroshio Extension region and its linkage with Aleutian atmospheric low pressure system. *Acta Oceanologica Sinica*, **35**, 24–37, https://doi.org/10.1007/s13131-016-0859-0.

Yu, P. L., C. Zhang, L. F. Zhang, X. Chen, Q. J. Zhong, M. H. Yang, and X. Li, 2020: An index for depicting the long-term variability of mesoscale eddy activity over the Kuroshio Extension region. *Atmosphere*, **11**, 792, https://doi.org/10.3390/atmos11080792.

Yuan, L., and Z. N. Xiao, 2017: The variability of the oceanic front in Kuroshio Extension and its relationship with the Pacific storm track in winter. *Chinese Journal of Atmospheric Sciences*, **41**, 1141–1155. (in Chinese with English abstract)

Zhang, C., H. L. Liu, C. Y. Li, and P. F. Lin, 2019: Impacts of mesoscale sea surface temperature anomalies on the meridional shift of North Pacific storm track. *International Journal of Climatology*, **39**, 5124–5139, https://doi.org/10.1002/joc.6130.

Zhang, C., H. L. Liu, J. B. Xie, P. F. Lin, C. Y. Li, Q. Yang, and J. Song, 2020a: North Pacific storm track response to the mesoscale SST in a global high-resolution atmospheric model. *Climate Dyn.*, **55**, 1597–1611, https://doi.org/10.1007/s00382-020-05343-x.

Zhang, R., J. B. Fang, and X.-Q. Yang, 2020b: What kinds of atmospheric anomalies drive wintertime North Pacific basin-scale subtropical oceanic front intensity variation? *J. Climate*, **33**, 7011–7026, https://doi.org/10.1175/JCLI-D-19-0973.1.

Zhou, G. D., and X. H. Cheng, 2022: Impacts of oceanic fronts and eddies in the Kuroshio-Oyashio Extension region on the atmospheric general circulation and storm track. *Adv. Atmos. Sci.*, **39**, 22–54, https://doi.org/10.1007/s00376-021-0408-4.

Zhu, W. J., and Y. Li, 2010: Inter-decadal variation characteristics of winter North Pacific storm tracks and its possible influencing mechanism. *Acta Meteorologica Sinica*, **68**, 477–486, https://doi.org/10.11676/qxxb2010.046. (in Chinese with English abstract)